GEOLOGY

Biomimetic mineral self-organization from silica-rich spring waters

Juan Manuel García-Ruiz,[1]* Elias Nakouzi,[2] Electra Kotopoulou,[1] Leonardo Tamborrino,[1†] Oliver Steinbock[2]

Purely inorganic reactions of silica, metal carbonates, and metal hydroxides can produce self-organized complex structures that mimic the texture of biominerals, the morphology of primitive organisms, and that catalyze prebiotic reactions. To date, these fascinating structures have only been synthesized using model solutions. We report that mineral self-assembly can be also obtained from natural alkaline silica-rich water deriving from serpentinization. Specifically, we demonstrate three main types of mineral self-assembly: (i) nanocrystalline biomorphs of barium carbonate and silica, (ii) mesocrystals and crystal aggregates of calcium carbonate with complex biomimetic textures, and (iii) osmosis-driven metal silicate hydrate membranes that form compartmentalized, hollow structures. Our results suggest that silica-induced mineral self-assembly could have been a common phenomenon in alkaline environments of early Earth and Earth-like planets.

INTRODUCTION

Living organisms and their biochemical products affect the crystallization of minerals, such as calcium carbonate and calcium phosphate, forming hybrid (organic-inorganic) composite materials, called biominerals, with shapes and textures significantly different from their purely inorganic counterparts (*1*, *2*). These properties were thought to be solely life-originated and are the rationale behind the use of morphology for detection of the oldest remnants of life on this planet and elsewhere (*3*–*5*). This view was challenged by the discovery that silica severely affects the crystallization of some carbonates inducing self-assembled inorganic-inorganic composite materials named "biomorphs" (*6*) that mimic the morphology and chemical signature of the putative microfossils found in Archean cherts (*7*–*9*) and the textures of some calcitic biominerals (*10*). This phenomenon of self-assembly occurs when carbonate minerals precipitate from silica-rich solutions under alkaline conditions, namely, in pH ranging from 9.5 to 12.5 (fig. S1), with a source of carbonate, such as atmospheric CO_2, in temperature ranging from 4° to 100°C.

Likewise, metal silicate hydrate (MSH) membranes, also known as silica gardens, precipitate upon reaction of silica-rich solutions and Me salt solutions (or solids) at a pH range of 11.4 to 12.5 (fig. S1), giving rise to membranous forms of life-like tubes or film-like structures with important catalytic properties (*11*, *12*). It is now known that these membranes show space compartmentalization, separating the inner and outer environments of distinct chemical and textural differences, and promote the selective catalysis of biologically relevant organic compounds, such as carboxylic acids, amino acids, and nucleobases in the presence of formamide, a well-spread organic molecule in the universe (*13*, *14*). To date, the synthesis of mineral self-assembly has been demonstrated with the use of laboratory model solutions (*15*), except for one case where calcium silicate hydrate membranes were obtained upon interaction of model alkaline fluids with granites (*16*).

Here, we have tested the precipitation of silica-carbonate biomorphs, calcium carbonate mesocrystals, and MSH membranes using natural water collected from the Ney spring (California, USA) (*17*, *18*). The alkaline Ney spring is located in Siskiyou County at the contact between the Trinity Ophiolite Complex and the albite-rich dacitic facies of the Tertiary basaltic-andesitic volcanic deposits. We measured a pH of 11.89 and a silica concentration of 4236 parts per million (fig. S1, table S1, and movie S1) that fulfill the requirements for silica-induced mineral self-assembly. The extremely high pH value of Ney's water arises from serpentinization (*18*), a geological process known to produce simple abiotic organic molecules, whereas the high-silica content is due to percolation through silica-rich volcanic rocks (see the Supplementary Materials for details).

RESULTS AND DISCUSSION

Figure 1 (A to K) shows the biomimetic structures of barium carbonate and silica, grown from the Ney water. Despite some structural differences, these materials conform to the main properties of silica-carbonate biomorphs (*6*, *19*, *20*). First, they exhibit smoothly curved surfaces that are not restricted to crystallographic geometries. For example, the Ney biomorphs grow irregular shapes with "appendages" that extend to millimeter-length scales (Fig. 1, A and B, and fig. S2, A and B) and thin sheets that often show topographic oscillations on the order of few micrometers (Fig. 1, E and F, and fig. S2, C and D), a signature of regular, laboratory-grown biomorphs (*19*). Perhaps the most conspicuous structures are the well-defined, twisted ribbons in Fig. 1 (C and D) that are highly reminiscent of microbial shapes. Note that all these structures form at pH values of 9.2 to 10.2, which are slightly lower than the pH range of regular biomorphs (fig. S1). By comparison, experiments at higher pH yield the rapid formation of conventional witherite crystals (*21*), because of the relatively high carbonate ion concentration in the Ney water.

The second defining feature of the Ney biomorphs is their hierarchical architecture that consists of thousands of elongated nanocrystals (Fig. 1G). Using autocorrelation image analyses (*19*), we determined the local orientation of these nanorods and found a high degree of nanocrystal alignment (Fig. 1H) that is comparable to biominerals, such as those found in sea urchins and mollusk shells (*22*). We also observed nanowires that form by the one-dimensional self-assembly of ~40-nm-diameter nanoparticles. However, we emphasize that these nanostructured

[1]Laboratorio de Estudios Cristalográficos, Instituto Andaluz de Ciencias de la Tierra, Consejo Superior de Investigaciones Científicas–Universidad de Granada, Avenida de las Palmeras 4, Armilla, Granada 18100, Spain. [2]Department of Chemistry and Biochemistry, Florida State University, Tallahassee, FL 32306–4390, USA.
*Corresponding author. Email: juanmanuel.garcia@csic.es
†Present address: MARUM–Center for Marine Environmental Sciences, University of Bremen, Leobener Strasse, 28359 Bremen, Germany.

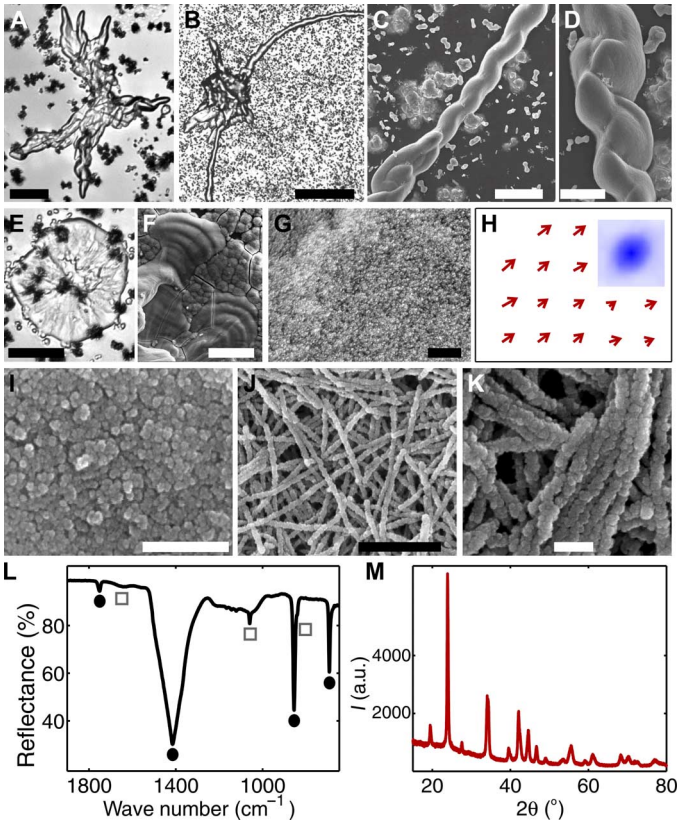

Fig. 1. Barium carbonate–based structures grown using the Ney water. Smoothly curved biomorphic shapes (**A** and **B**), helical structures (**C** and **D**), and flat sheets (**E**) showing oscillatory features (**F**). (**G** and **I**) Higher-resolution images reveal the nanocrystals that constitute the biomorphs. (**H**) Nanocrystal alignment direction obtained from the correlation analyses of the micrograph in (G); inset shows a representative correlation map. (**J** and **K**) Some of the structures consist of nanowires. (**L**) Infrared spectrum shows silica (gray squares) and crystalline barium carbonate (black circles) peaks. (**M**) X-ray diffraction (XRD) diffractogram with the characteristic witherite peaks. a.u., arbitrary units. Scale bars, 50 μm (A), 200 μm (B), 10 μm (C), 2 μm (D), 20 μm (E and F), 1 μm (G and J), and 200 nm (I and K).

materials are produced by simple, inorganic reactions that, as demonstrated by our results, can plausibly occur in natural water samples. Third, the chemical and crystallographic properties of the biomorphs formed in the Ney water also match those displayed by biomorphs obtained from model solutions (Fig. 1, L and M) (*6*). The structures consist predominantly of crystalline barium carbonate (69 ± 2%) and amorphous silica (27 ± 3%). Note that this rich variety of morphologies compared to typical biomorphs can be ascribed to the influence of metals and anions (*23*) derived from fluid-rock interactions in the Ney water.

In the second set of experiments, we studied the crystallization of calcium carbonate in the Ney water by diluting, to decrease the pH and the silica concentration, and by adding calcium ions. The dilution of the spring water naturally occurs in geological scenarios. At a pH value of 9, the obtained crystals are {104} calcite rhombohedra with slightly modified euhedral morphologies (Fig. 2A). As the pH value is progressively increased, new crystal forms appear, such as scalenohedron and nonsingular faces tautozonal to the *c* axis (Fig. 2B and fig. S3, A and B). At pH values greater than 10.5, the crystals grow by aggregation of platelet-like blocks with no trace of the original flat faces but retaining the point symmetry group (−32/m) of the calcite crystal structure (Fig. 2, C and D). This continuous evolution from modified rhombohedra to nanostructured assemblies is accompanied by an increase in silica content from 6 ± 2% to 36 ± 6%. Note that similar morphologies were obtained by Kulak *et al.* (*24*) for $CaCO_3$ crystallization in the presence of double-hydrophilic block copolymers. In this context, silica performs an analogous role to the polymeric additives in directing the crystallization mechanism, although the details at molecular level might not be identical in both cases. Even more surprisingly, the Ney waters assemble highly ordered architectures from building blocks with different crystal habits and sizes. For example, Fig. 2H shows a polycrystalline assembly with threefold rotational symmetry that is itself composed of subunits shaped like three-pointed stars (Fig. 2I) (*25*). By comparison, the structures in Fig. 2 (J and K) consist of nanoplatelets stacked in a staggered, brick-like fashion (*26*), from which micrometer-sized spicules extend with a well-defined orientation. The nanoplatelets consist of hundreds of spherical nanoparticles (fig. S3, C and D), suggesting growth by oriented particle attachment (*27*–*30*). Concomitant with these calcitic microstructures, the presence of vaterite spherulitic structures at pH values between 9.5 and 11 was detected by micro-Raman spectroscopy (Fig. 2, E and F). These results are further supported by infrared spectroscopy and x-ray diffraction measurements (fig. S4).

In the third set of experiments, we grew MSH membranes, the so-called silica gardens, from the natural Ney water. Following the classical protocol, we immersed soluble pellets of Co(II), Fe(II), Fe(III), Cu(II), Mg(II), Ni(II), and Zn(II) salts in the Ney water and observed the reaction. In the case of Co(II) and Fe(II), we obtained typical hollow tubes (Fig. 3 and figs. S5 and S6) similar to those produced with model solutions. These structures reproduce a key feature of classical silica gardens: textural and compositional gradients across the membrane (*31*, *32*). In particular, the outer surface of the MSH membrane, facing toward the silica-rich Ney water, is smooth and homogeneous (Fig. 3, B, C, G, and H), while the inner surface consists of microrosettes and nanoglobules (Fig. 3, C and H). Moreover, we observed that the outer membrane surface is rich in silica and metal silicates, whereas the inner surface is rich in metal (oxy)hydroxides (Fig. 3, D, E, I, and J). The formation of tubules in the Ney water is relatively slow (hours) (figs. S5 and S6) compared to the classical experiments (within seconds to minutes) (*31*). The latter result can be attributed to the smaller difference in ionic strength between the inner and outer solution for the case of the Ney experiments, reducing the strength of the osmotically driven force. The experiments performed with Fe(III), Cu, and Zn salts released a large amount of CO_2 bubbles, leading to the premature bursting of the forming MSH membrane (see movies S2 to S4). This behavior (i) increases the availability of the surface area of both sides of the membranes and (ii) quickly releases newly forming molecules. Both observations are particularly interesting to enhance the role of membranous MSH structures as catalysts in geochemical scenarios (*12*, *13*).

CONCLUSIONS

In conclusion, crystallization patterns observed in alkaline natural waters confirm the ability of silica to imitate the role of organic matter in biomineralization and moreover suggest that silica-induced mineral self-assembly could have been a common phenomenon on primitive Earth and Earth-like planets, where alkaline environments are thought to be widespread. The structural complexity obtained from simple precipitation reactions in the natural Ney water further blurs the boundaries between geochemical and biological morphologies that, not too long ago, were perceived as sharp and well defined. Finally,

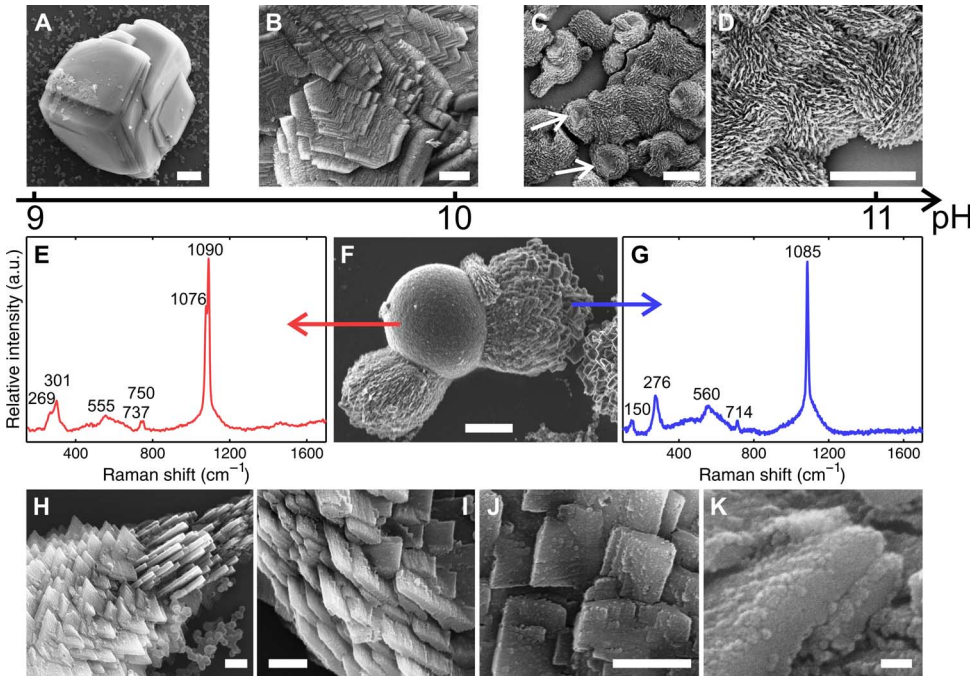

Fig. 2. Calcium carbonate–based structures. (**A** to **D**) Morphological trend from classical rhombohedra to nanostructured aggregates with increasing pH. (**E** to **G**) Scanning electron microscopy (SEM) image (F) of a crystal aggregate showing two distinctive morphologies and the Raman spectrum of the calcitic (E) and vateritic (G) domains of the crystal aggregate. (**H** and **K**) Hierarchical structures of stacked nanoplatelets consisting of nanoparticles. Scale bars, 20 μm (A and C), 5 μm (B, D, and F), 2 μm (H and I), 500 nm (J), and 50 nm (K).

the proof that MSH membranes can be readily formed in waters derived from serpentinization supports the geochemical plausibility of the role of MSH membranes in catalyzing the building blocks of life from simple reactions, such as formamide condensation (*13*, *14*).

MATERIALS AND METHODS

Sampling and geological setting

The sampling campaign took place on 10 and 11 August 2015 in a Ney spring, located at coordinates 41°15′43″N and 122°19′54″W. Samples were collected in plastic bottles. The pH value of the water of the Aqua de Ney spring was measured to be 11.9 in situ. The temperature of the water in the Ney well was 14.5°C, whereas that of the water of the creek was 15.6°C.

The Ney springs belong to an abandoned spa called Aqua de Ney at the Ney Creek, a tributary of the Sacramento River, in the eastern Klamath Mountains (Siskiyou County, northern California, USA), 8 km south of Mount Shasta (fig. S1 and movie S1). The springs are located about 300 m downstream of the Fairy Falls, and they can be accessed following the Ney Springs Canyon Trail. Only the spring closer to the shore of the creek pours alkaline water. This alkaline spring is today a well, built in a hexagonal shape, located a couple of meters above the creek. The water leaves the well through an underground connection to another artificial, circular pool closer to the creek that was used as a footbath in the spa created by John Ney in the late 19th century.

Ney springs are located in the geological context of the Ordovician Trinity subterrane, an east-dipping ultramafic sheet composed of serpentinized tectonitic peridotite (also known as Trinity Ophiolite) with gabbro-dioritic intrusions (*17*, *18*, *33*–*35*). The geological scenario is completed by the overlain Devonian-Mississippian volcanic and sedimentary units (Redding subterrene), the Jurassic granitic plutons, and the Cascade Range Eocene-Quaternary sequence, comprising volcanic and sedimentary deposits (fig. S1). The Tertiary sequence outcrops with a deeply weathered albite-rich dacitic facies on the southern side of the canyon, at the level of the Ney springs. The alkaline Ney spring is located in the contact of the Trinity Ophiolite Complex and the albite-rich dacitic facies of the Tertiary basaltic-andesitic volcanic deposits (*33*–*35*).

Major and minor elemental composition, in situ and ex situ pH values, and temperature of the water as well as comparison with previous chemical analysis (*17*, *18*) are indicated in table S1. There are two noticeable properties: first, the alkaline character of the water and, second, the very high silica concentration, the highest value reported in the literature. It has previously been suggested (*18*, *34*) that the alkaline character and the high pH of the water result from serpentinization processes occurring during the streaming of the water through fractions of the ultramafic rocks of the ophiolite complex. The extraordinary enrichment in silica could be explained by the flowing of the alkaline water through the dacitic-andesitic-basaltic rocks, as a result of the dissolution of silica and silica-rich minerals under high pH conditions. These high pH values and the high silica concentration make the Ney spring the best contemporary candidate, so far, to demonstrate the geochemical plausibility of nanomineral self-assembly.

Hydrochemistry

We performed chemical analysis of the Aqua de Ney water with a range of quantitative instruments. The SiO_2, Mg^{2+}, Ca^{2+}, Ba^{2+}, Sr^{2+}, Na^+, Li^+, K^+, B^{n+}, and Mo^{n+} concentrations were measured using a PerkinElmer 7300 inductively coupled plasma (ICP) atomic emission spectrometer operating in the dual view mode. A second measurement of the Ba^{2+}, Li^+, and Mo^{n+} concentrations was performed using a Thermo X7 ICP-MS (mass spectrometer. Furthermore, we determined the anion concentrations (Cl^-, SO_4^{2-}, CO_3^{2-}, and HCO_3^-) using ion chromatography. The

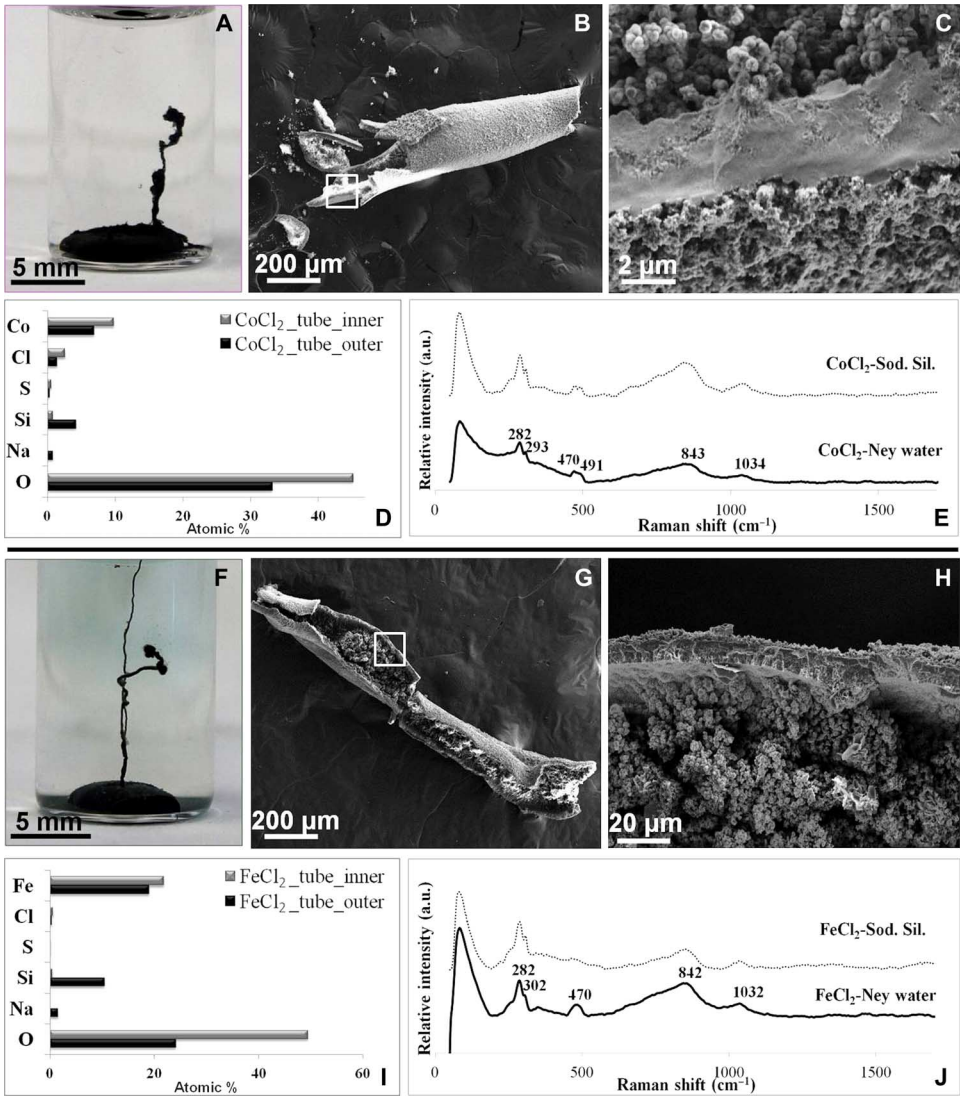

Fig. 3. Silica gardens. (**A** to **C**) MSH tubular membranes produced by reaction of the Co salt pellet with the Ney water. (**D**) Comparative histogram of the chemical composition [energy-dispersive x-ray spectroscopy (EDX)] of the inner part (gray) and the outer part (black) of the Co-based tube. (**E**) Raman spectra of the Co-based tubes produced in Ney water (black) and laboratory sodium silicate (Sod. Sil.) solutions (gray). (**F** to **H**) MSH tubular membrane produced by the reaction of the Fe(II) salt pellet with the Ney water. (**I**) Comparative histogram for the chemical composition (EDX) of the inner part (gray) and the outer part (black) of the Fe-based tube. (**J**) Raman spectra of the Fe-based tubes produced in Ney water (black curve) and laboratory sodium silicate solutions (gray curve).

conductivity and fluoride ion concentration were determined using a Mantech PC-Titrate autotitrator system. However, the exceedingly high alkalinity of the Aqua de Ney water samples could not be measured using this instrument. Therefore, we performed a manual titration of three aliquots of the Aqua de Ney water with 0.1 N (0.05 M) of sulfuric acid. The water samples required 166 ± 3 ml of the titrant to reach a pH value of 4.5. Notice that this value is not solely indicative of the carbonate ion concentration, because the high silica concentration also contributes to the alkalinity.

Growth of biomorphs of barium carbonate and biomimetic calcium carbonate

The barium carbonate and calcium carbonate crystallization experiments were performed according to the gas diffusion (*7*) and single-phase methods (*31*). For this purpose, we prepared stock solutions of 0.1 M barium chloride dihydrate and calcium carbonate dihydrate (Fisher Scientific) using ultrapure water (Barnstead EASYpure UV). We then prepared the crystallization solutions by diluting the Aqua de Ney water samples by a factor of 10, 20, or 40 times and by adding 1.0, 2.5, and 5.0 mM of the alkaline earth metal ion. The pH was adjusted to an initial value of 9 to 11 using a few drops of 0.1 M hydrochloric acid or sodium hydroxide. For the gas diffusion experiments, 4-ml aliquots of this solution were placed into ventilated Greiner Bio-One petri dishes that allow the diffusion of atmospheric carbon dioxide. For the single-phase experiments, we used ~10-ml aliquots of the solution that almost completely filled the reaction containers, leaving no space for a solution-gas interface. The petri dishes were then covered and tightly sealed using multiple layers of Parafilm. Note that in this method, we purged the required volumes of distilled water and metal ion solution with nitrogen gas before mixing to significantly reduce the predissolved carbon dioxide.

The optical microscopy images of the crystal aggregates were acquired using a Nikon Elements Ti inverted microscope coupled to a Photometrics CoolSNAP HQ2 camera. To obtain the electron micrographs, we used a FEI Nova 400 field-emission SEM (FESEM) operating at 5 to 15 kV. The molar percent chemical composition was measured using an INCA EDX detector. For these measurements, the crystals were grown on glass substrates that could be retrieved, rinsed, and coated with thin iridium films. Furthermore, we conducted the powder XRD (PXRD) measurements using PANalytical X'Pert PRO with a copper x-ray source and operating at a scan speed of 0.02°/s for a 2θ range of 10° to 80°. The infrared spectra were collected using a PerkinElmer Spectrum 100 Fourier transform infrared spectrometer functioning in attenuated total reflectance mode.

The local orientation of the nanorods forming the biomorphs was determined using an image correlation analysis. This method is based on the two-dimensional autocorrelation function of gray-level SEM micrographs of the crystal aggregates. Specifically, the correlation decay was calculated as the image was shifted by Δx in x direction and Δy in y direction. Similar analyses were carried out for nonoverlapping boxes of 200 × 200 pixels of the same image and yielded local autocorrelation maps $c(\Delta x,\Delta y)$. As expected, the correlation is equivalent to unity for $(\Delta x,\Delta y) = (0,0)$ and decays rapidly in all directions but persists slightly longer in the direction of anisotropy. We obtained this orientation by fitting an ellipse to the $c = 0.2$ contour and measuring the length of its short (that is, semiminor) and long (semimajor) axes. The nanorod orientation was thus given by the long ellipse axis and was mapped as a vector field in Fig. 1J. The individual vector lengths provide semiquantitative measures of the quality of the correlation and, hence, the degree of nanorod alignment. Finally, we used arrowheads to tentatively assign the biomorph growth direction.

Precipitation of MSH membranes

A sample of Ney water (3 ml) was poured into 4-ml glass vials, whereas Me salt pellets of $CoCl_2{\bullet}6H_2O$, $Fe_2(SO_4)_3{\bullet}9H_2O$, $FeCl_2{\bullet}4H_2O$, $CuCl_2{\bullet}2H_2O$, $MgSO_4$, $NiCl_2{\bullet}6H_2O$, and $ZnCl_2$ were placed, separately, in the Ney solution (pellets were prepared using an agate mortar, until reaching the powder fraction, and a press of up to 10 metric tons). The experiments were conducted (i) under ambient conditions, (ii) inside the glove box (N_2 atmosphere), and (iii) at a temperature of 60°C. Here, we discuss MSH membrane formation under ambient conditions. Detailed description of the results from the different experiments will be provided in a following publication.

Following the formation of the MSH tubular membranes and the termination of the phenomenon, the membranes were studied ex situ under a FESEM equipped with an Oxford EDX to examine their texture and chemical composition. Also, PXRD was performed, to identify the mineral crystalline phases of the membranes, with the X'Pert PRO MPD (PANalytical) diffractometer that was powered by a Philips PW3040/60 x-ray generator (Cu-K_α) and fitted with an X'Celerator detector at an acceleration voltage of 40 kV and a current of 40 mA. Phase identification was carried out with the HighScore Plus software (PANalytical) and the American Mineralogist Crystal Structure Database. Raman spectra were recorded using a HORIBA Jobin Yvon LabRAM high-resolution ultraviolet–visible light spectrometer equipped with an Olympus BX41 optical microscope with binocular and Koehler illumination and a charge-coupled device detector at an excitation wavelength of 532 nm (frequency-doubled neodymium-doped yttrium-aluminum-garnet laser).

In the case of the gas production upon reaction of the Fe(III), Cu(II), and Zn(II) salts with the Ney water, gas chromatography (GC)–MS was used to identify the gas phase using an Agilent Varian (now Bruker) 450-GC 240-MS ion trap mass spectrometer (40-ml manual injection, gas-type syringe). For the measurement, standard air samples as well as blank samples of the Ney solution were used (fig. S7).

SUPPLEMENTARY MATERIALS

Supplementary material for this article is available at http://advances.sciencemag.org/cgi/content/full/3/3/e1602285/DC1

table S1. Comparative chemical analysis of the Ney water by Feth *et al.* (*17*), Barnes *et al.* (*18*), and this study.

fig. S1. Sampling and geological setting of the Ney spring.

fig. S2. Electron micrographs of barium-based self-assembled structures.

fig. S3. Electron micrographs of calcium-based structures grown at pH 10.5.

fig. S4. XRD pattern and infrared spectrum of the calcium-based structures.

fig. S5. MSH tubular membrane produced by reaction of the Co salt ($CoCl_2{\bullet}6H_2O$) pellet with the Ney water.

fig. S6. MSH tubular membrane produced by the reaction of the Fe(II) salt pellet ($FeCl_2{\bullet}4H_2O$) with the Ney water.

fig. S7. Chromatograms indicating the production of CO_2(g) upon reaction of the pellets with the Ney water.

movie S1. The alkaline Ney spring showing the hexagonal fabric of the well and the circular hole for feet treatment that were in use during the working time of the Aqua de Ney Spa, inactive since 1941.

movie S2. CO_2 bubbling and bursting of reaction products of the $Fe_2(SO_4)_3{\bullet}9H_2O$ pellet and the sodium silicate solution.

movie S3. CO_2 bubbling and bursting of reaction products of the $CuCl_2{\bullet}2H_2O$ pellet and the sodium silicate solution.

movie S4. CO_2 bubbling and bursting of reaction products of the $ZnCl_2$ pellet and the sodium silicate solution.

REFERENCES AND NOTES

1. H. A. Lowenstam, S. Weiner, *On Biomineralization* (Oxford Univ. Press, 1989).
2. P. Behrens, E. Bauerlein, *Handbook of Biomineralization: Biomimetic and Bioinspired Chemistry* (Wiley, 2009).
3. R. Buick, Microfossil recognition in Archean rocks: An appraisal of spheroids and filaments from a 3500 m.y. old chert-barite unit at North Pole, Western Australia. *Palaios* **5**, 441–459 (1990).
4. F. Stalport, P. Coll, M. Cabane, A. Person, R. Navarro-González, F. Raulin, M. J. Vaulay, P. Ausset, C. P. McKay, C. Szopa, J. Zarnecki, Search for past life on Mars: Physical and chemical characterization of minerals of biotic and abiotic origin: Part 1 - calcite. *Geophys. Res. Lett.* **32**, L23205 (2005).
5. M. D. Brasier, O. R. Green, A. P. Jephcoat, A. K. Kleppe, M. J. Van Kranendonk, J. F. Lindsay, A. Steele, N. V. Grassineau, Questioning the evidence for Earth's oldest fossils. *Nature* **416**, 76–81 (2002).
6. M. Kellermeier, H. Cölfen, J. M. García-Ruiz, Silica biomorphs: Complex biomimetic hybrid materials from "Sand and Chalk". *Eur. J. Inorg. Chem.* **2012**, 5123–5144 (2012).
7. J. M. García-Ruiz, A. Carnerup, A. G. Christy, N. J. Welham, S. T. Hyde, Morphology: An ambiguous indicator of biogenicity. *Astrobiology* **2**, 353–369 (2002).
8. J. M. García-Ruiz, S. T. Hyde, A. M. Carnerup, A. G. Christy, M. J. Van Kranendonk, N. J. Welham, Self-assembled silica-carbonate structures and detection of ancient microfossils. *Science* **302**, 1194–1197 (2003).
9. J. M. García-Ruiz, Carbonate precipitation into alkaline silica-rich environments. *Geology* **26**, 843–846 (1998).
10. J. M. García-Ruiz, Geochemical scenario for the precipitation of biomimetic inorganic carbonates, in *Carbonate Sedimentation and Diagenesis in the Evolving Precambrian World*, J. P. Grotzinger, N. P. James, Eds. (SEPM Special Publication, ed. 67, 2000), pp. 75–89.
11. F. Glaab, M. Kellermeier, W. Kunz, E. Morallon, J. M. García-Ruiz, Formation and evolution of chemical gradients and potential differences across self-assembling inorganic membranes. *Angew. Chem. Int. Ed. Engl.* **51**, 4317–4321 (2012).
12. L. M. Barge, S. S. S. Cardoso, J. H. E. Cartwright, G. J. T. Cooper, L. Cronin, A. De Wit, I. J. Doloboff, B. Escribano, R. E. Goldstein, F. Haudin, D. E. H. Jones, A. L. Mackay, J. Maselko, J. J. Pagano, J. Pantaleone, M. J. Russell, C. I. Sainz-Diaz, O. Steinbock, D. A. Stone, Y. Tanimoto, N. L. Thomas, From chemical gardens to chemobrionics. *Chem. Rev.* **115**, 8652–8703 (2015).

13. R. Saladino, G. Botta, B. M. Bizzarri, E. Di Mauro, J. M. García-Ruiz, A global scale scenario for prebiotic chemistry: Silica-based self-assembled mineral structures and formamide. *Biochemistry* **55**, 2806–2811 (2016).
14. D. Niether, D. Afanasenkau, J. K. G. Dhont, S. Wiegand, Accumulation of formamide in hydrothermal pores to form prebiotic nucleobases. *Proc. Natl. Acad. Sci. U.S.A.* **113**, 4272–4277 (2016).
15. E. Nakouzi, O. Steinbock, Self-organization in precipitation reactions far from the equilibrium. *Sci. Adv.* **2**, e1601144 (2016).
16. H. Satoh, K. Tsukamoto, J. M. García-Ruiz, Formation of chemical gardens on granitic rock: A new type of alteration for alkaline systems. *Eur. J. Mineral.* **26**, 415–426 (2014).
17. J. H. Feth, S. M. Roogers, C. E. Roberson, Aqua de Ney, California, a spring of unique chemical character. *Geochim. Cosmochim. Acta* **22**, 75–76 (1961).
18. I. Barnes, J. B. Rapp, J. R. O'Neil, R. A. Sheppard, A. J. Gude III, Metamorphic assemblages and the direction of flow of metamorphic fluids in four instances of serpentinization. *Contrib. Mineral. Petrol.* **35**, 263–276 (1972).
19. E. Nakouzi, P. Knoll, O. Steinbock, Biomorph growth in single-phase systems: Expanding the structure spectrum and pH range. *Chem. Commun.* **52**, 2107–2110 (2016).
20. J. M. García-Ruiz, E. Melero-Garcia, S. T. Hyde, Morphogenesis of self-assembled nanocrystalline materials of barium carbonate and silica. *Science* **323**, 362–365 (2009).
21. J. Eiblmeier, S. Dankesreiter, A. Pfitzner, G. Schmalz, W. Kunz, M. Kellermeier, Crystallization of mixed alkaline-earth carbonates in silica solutions at high pH. *Cryst. Growth Des.* **14**, 6177–6188 (2014).
22. S. Mann, *Biomineralization: Principles and Concepts in Bioinorganic Materials Chemistry* (Oxford Univ. Press, 2001).
23. E. Nakouzi, R. Rendina, G. Palui, O. Steinbock, Effect of inorganic additives on the growth of silica–carbonate biomorphs. *J. Cryst. Growth* **452**, 166–171 (2016).
24. A. N. Kulak, P. Iddon, Y. Li, S. P. Armes, H. Cölfen, O. Paris, R. M. Wilson, F. C. Meldrum, Continuous structural evolution of calcium carbonate particles: A unifying model of copolymer-mediated crystallization. *J. Am. Chem. Soc.* **129**, 3729–3736 (2007).
25. H. Imai, T. Terada, S. Yamabi, Self-organized formation of a hierarchical self-similar structure with calcium carbonate. *Chem. Commun.* **2003**, 484–485 (2003).
26. B. J. F. Bruet, H. J. Qi, M. C. Boyes, R. Panas, Nanoscale morphology and indentation of individual nacre tablets from the gastropod mollusc *Trochus Niloticus*. *J. Mater. Res.* **20**, 2400–2419 (2005).
27. S. Domínguez-Bella, J. M. García-Ruiz, Agregados cristalinos de morfologia inducida de carbonato cálcico. Secuencia morfológica a pH 10. *Bol. R. Soc. Esp. Hist. Nat. Secc. Geol.* **81**, 173–185 (1983).
28. J. J. De Yoreo, P. U. P. A. Gilbert, N. A. J. M. Sommerdijk, R. L. Penn, S. Whitelam, D. Joester, H. Zhang, J. D. Rimer, A. Navrotsky, J. F. Banfield, A. F. Wallace, F. M. Michel, F. C. Meldrum, H. Cölfen, P. M. Dove, Crystallization by particle attachment in synthetic, biogenic, and geologic environments. *Science* **349**, aaa6760 (2015).
29. R.-Q. Song, H. Cölfen, Mesocrystals—Ordered nanoparticle superstructures. *Adv. Mater.* **22**, 1301–1330 (2010).
30. D. Vielzeuf, N. Floquet, D. Chatain, F. Bonneté, D. Ferry, J. Garrabou, E. M. Stolper, Multilevel modular mesocrystalline organization in red coral. *Am. Mineral.* **95**, 242–248 (2010).
31. W. Kellermeier, F. Glaab, E. Melero-García, J. M. García-Ruiz, Experimental techniques for the growth and characterization of silica biomorphs and silica gardens, in *Methods in Enzymology*, vol. 532 of *Research Methods in Biomineralization Science*, J. J. De Yoreo, Ed. (Academic Press, 2013), pp. 225–256.
32. J. J. Pagano, S. Thouvenel-Romans, O. Steinbock, Compositional analysis of copper–silica precipitation tubes. *Phys. Chem. Chem. Phys.* **9**, 110–116 (2007).
33. M. Brouxel, H. Lapierre, Geochemical study of an early Paleozoic island-arc-back-arc basin system. Part 1: The Trinity Ophiolite (northern California). *Geol. Soc. Am. Bull.* **100**, 1111–1119 (1988).
34. I. Barnes, J. R. O'Neil, The relationship between fluids in some fresh alpine-type ultramafics and possible modern serpentinization, western United States. *Geol. Soc. Am. Bull.* **80**, 1947–1960 (1969).
35. W. P. Irwin, "Geologic map of the Klamath Mountains, California and Oregon" (Miscellaneous Investigations Series Map I-2148, U.S. Geological Survey, 1994); https://ngmdb.usgs.gov/Prodesc/proddesc_10149.htm.

Acknowledgments: We thank I. G. Tschuschke (Centro de Instrumentación Científica–University of Granada) for assistance during the FESEM investigation and R. N. Gómez (Estación Experimental del Zaidín–Consejo Superior de Investigaciones Científicas) for assistance in gas chromatography. E.N. acknowledges the Mineralogical Society of America and the International Centre for Diffraction Data. **Funding:** We acknowledge funding from the European Research Council under the European Union's Seventh Framework Programme (FP7/2007-2013)/European Research Council grant agreement no. 340863 (Prometheus). This work was also supported by the NSF under grant no. 1609495. **Author contributions:** E.N. and E.K. performed the experiments, analyzed the materials, discussed the results, and wrote the paper. L.T. contributed to the geological setting. O.S. analyzed and discussed the results. J.M.G.-R. conceived the work, sampled the water, analyzed and discussed the results, and wrote the paper. **Competing interests:** The authors declare that they have no competing interests. **Data and materials availability:** All data needed to evaluate the conclusions in the paper are present in the paper and/or the Supplementary Materials. Detailed descriptions of materials and methods, geological setting, fluid chemistry, and spectroscopic characterization are also in the Supplementary Materials. Additional data related to this paper may be requested from the authors.

Submitted 19 September 2016
Accepted 9 February 2017
Published 17 March 2017
10.1126/sciadv.1602285

Citation: J. M. García-Ruiz, E. Nakouzi, E. Kotopoulou, L. Tamborrino, O. Steinbock, Biomimetic mineral self-organization from silica-rich spring waters. *Sci. Adv.* **3**, e1602285 (2017).

ScienceAdvances
AAAS

Biomimetic mineral self-organization from silica-rich spring waters

Juan Manuel García-Ruiz, Elias Nakouzi, Electra Kotopoulou, Leonardo Tamborrino and Oliver Steinbock (March 17, 2017)

Sci Adv 2017, 3:.
doi: 10.1126/sciadv.1602285